IET Power Electronics

Research Article

IET Journals
The Institution of Engineering and Technology

High-performance unified power quality conditioner using non-linear sliding mode and new switching dynamics control strategy

ISSN 1755-4535
Received on 12th December 2014
Revised 25th January 2017
Accepted on 20th February 2017
E-First on 16th March 2017
doi: 10.1049/iet-pel.2014.0881
www.ietdl.org

Rajesh Kumar Patjoshi[1] ✉, *Kamalakanta Mahapatra*[2]

[1]*Electronics and Communication Engineering Department, KL University, Vaddeswaram, Guntur, India*
[2]*Electronics and Communication Engineering Department, National Institute of Technology, Rourkela, India*
✉ *E-mail: rajeshpatjoshi1@gmail.com*

Abstract: In this study, a non-linear sliding mode control (NLSMC) and new switching dynamics control strategy have been proposed for a unified power quality conditioner (UPQC) to improve the power quality problem in power system distribution network. The proposed non-linear sliding surface reflects the controlling action of the DC-link capacitor voltage with a variation of the system's damping ratio and permits the DC-link voltage to obtain a low overshoot and small settling time. This NLSMC technique combines with a novel synchronous-reference frame (SRF) control technique for generation of a rapid and stable reference signal for both shunt and series converters. A new switching dynamics control strategy has been designed for the voltage source converters of UPQC and this design helps in the reduction of band violation of the hysteresis band as well as improvement in the tracking behaviour of UPQC during grid perturbations. Consequently, NLSMC-SRF technique along with new switching strategy in UPQC provides an effective compensator for voltage/current harmonics, sag/swell, voltage unbalance and interruptions. The proposed control strategy of UPQC is validated through MATLAB/SIMULINK, followed by the experimental system using real-time hardware-in-the-loop. Adequate results are reported after a comparative assessment with the conventional proportional–integral and hysteresis controller.

1 Introduction

Nowadays, power quality (PQ) issue is one of the major problems due to growing usage of non-linear power electronics loads and equipment in residences as well as in industries [1] has led to create harmonics in voltage and current. In addition, various network faults and switching of capacitor banks also create PQ issues, such as voltage sag/swell, voltage unbalance and voltage interruptions. Unified PQ conditioner (UPQC) is a custom power device, which is one of the promising solutions for mitigating these PQ issues. A general block diagram of UPQC is depicted in Fig. 1*a* consisting of shunt and series converters coupled through a common DC-link capacitor. Generally shunt converter is connected in parallel with loads through the coupling inductor L_{shf} to compensate all current related problems [2] whilst series converter is connected in series with line through ac filter (R_{sf}, L_{sf} and C_{f}), switching resistor R_g and series transformer for compensating all voltage related problems [3].

DC-link voltage regulation is one of the essential methodologies in UPQC and various methods such as proportional–integral (PI), PI–derivative and fuzzy controllers [4–6] have been proposed for controlling the DC-link voltage. These controllers fail to regulate the DC-link voltage during fast transient conditions of system load and system uncertainty condition due to the failure of system components in the power disturbance network. Hence, the DC-link voltage of the UPQC can significantly deviate from its reference value and takes finite time interval to return to its original value, resulting in performance degradation of UPQC compensation process. To ensure high performance UPQC system, the DC-link voltage should settle quickly with a low overshoot. It is a well-comprehended certainty that a low overshoot can be accomplished with high settling time and vice versa, which is not desirable in UPQC as DC-link capacitor voltage can control the operation of both shunt and series converters. The proposed non-linear sliding mode control (NLSMC) solves this particular problem, which is a combination of composite non-linear feedback (CNF) [7, 8] and sliding mode control (SMC) techniques [9].

Recently, various studies have been carried out in order to consolidate the advantages of CNF and SMC techniques. This combination of CNF and SMC is one of the preferable choices for a system with uncertainties and disturbances [10, 11]. It was shown in [12] that NLSMC has potential for match perturbations, better tracking performance, low overshoot and low settling time by varying the system's closed-loop damping ratio in its non-linear surface. Initially, the non-linear surface preserves the damping ratio at a low value and regularly varies it towards an ultimate high value to guarantee fast response, when DC-link voltage approaches a set point. Thus, this control algorithm provides an enhanced performance for regulating the DC-link voltage of UPQC. Further, the performance of UPQC depends upon how quickly and how accurately reference signal is extracted during power system dynamic condition. Hence, we consider NLSMC-SRF (synchronous-reference frame) reference generation technique by combining both NLSMC and SRF techniques. This method extracts the peak amplitude of source current and fundamental positive-sequence signal accurately during power system dynamic condition and generates the reference signal quickly.

Reference signal tracking control plays an essential role in PQ improvement, generally hysteresis band (HB) current and voltage controllers [13, 14] are utilised for tracking a specified reference current and voltage for generation of pulse-width modulation (PWM) signal for controlling both converters. The HB control (HBC) method has fast response and ease in implementation in compared with other control strategies like triangular carrier PWM [15] and space-vector modulation (SVM) technique [16]. In contrast, HBC exhibits undesirable features such as band violation during grid perturbation and uneven switching frequency which gives rise to acoustic noise causing difficulty in designing of LC filter for series converter. As a result, poor compensation and serious filter currents are brought into notice. Considering above facts taken into account, a proper switching dynamics for HB needs to be developed, through which a simpler band calculation, less band violation, better tracking performance of reference signal and better injection capability of compensating current as well as compensating voltage at point of common coupling of power distribution network can be achieved.

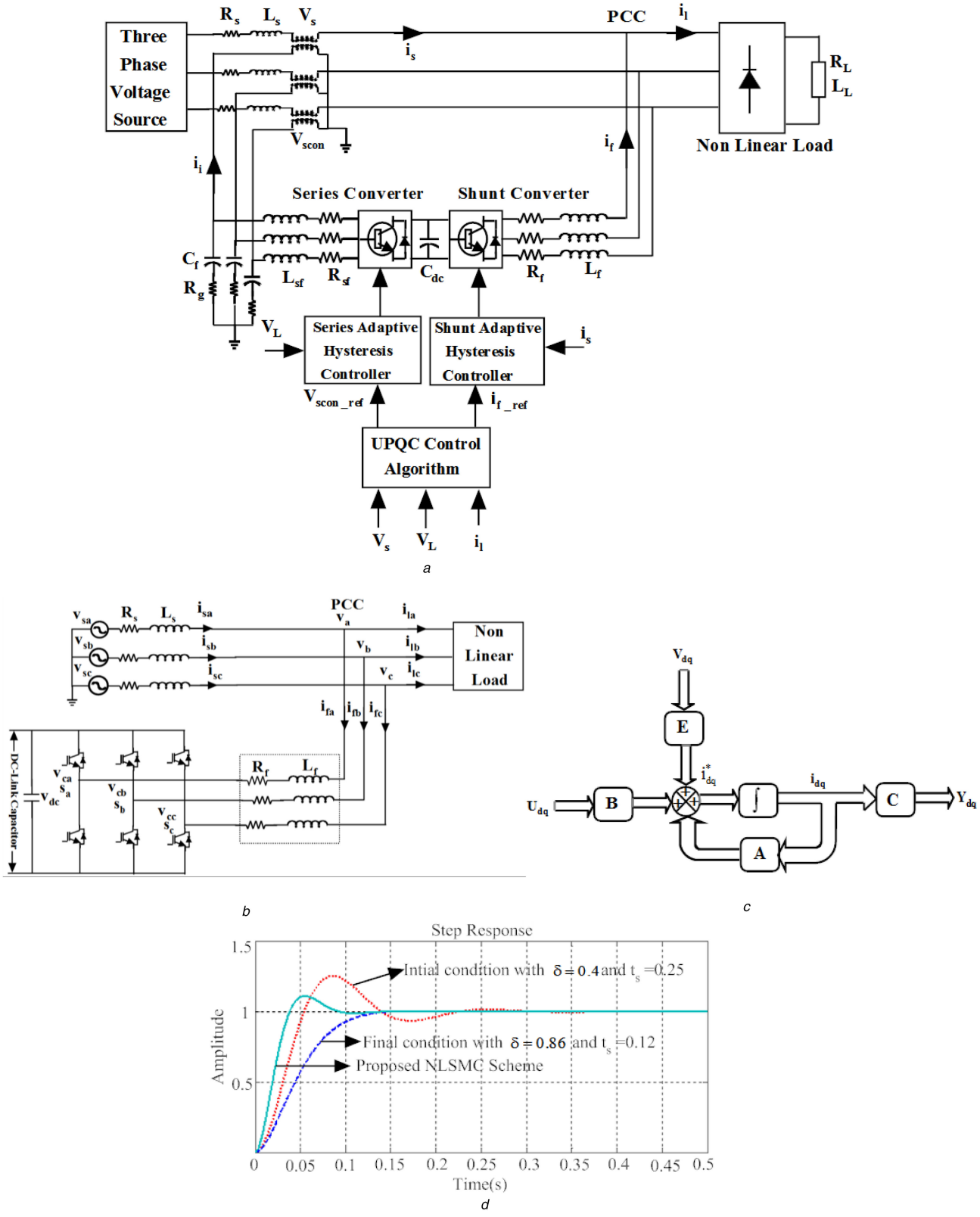

Fig. 1 *System configuration and response of UPQC*

(a) General block diagram representation of UPQC, ***(b)*** Schematic diagram of shunt converter, ***(c)*** System representation of part of the plant model of shunt converter, ***(d)*** Step response of the proposed method with initial and final conditions of damping ratio and settling time

Therefore, a new switching dynamics for HB has been proposed here and the formulation of HB depends upon the DC-link voltage regulation as well as reference signal generation. Thus, the proposed NLSMC-SRF-based new switching dynamic for HB can effectively eliminate PQ issues like current/voltage harmonics, voltage sag/swell, voltage unbalance and voltage interruptions during any operating conditions of power system perturbations. The proposed control technique is validated through extensive simulation and real-time experimental studies accomplished by using hardware-in-the-loop (HIL) system in OPAL-RT simulator (OP5600) with OP5142 Xilinx SPARTAN-3(3xc3s5000) field programmable gate array (FPGA) processor for user interconnection. A comparative assessment has been performed between proposed control strategy, conventional PI controller and fixed-HBC technique.

2 Design of NLSMC scheme for DC-link voltage regulation

Generally the shunt converter of UPQC is responsible for DC-link voltage regulation. Thus the proposed NLSMC scheme is designed for a shunt converter for DC-link voltage regulation. Schematic diagram of the shunt voltage source converter (VSC) is depicted in Fig. 1*b*. The conventional dynamic equations of plant model in a *d*–*q* frame are presented in (1) and (2). The plant system representation model is depicted in Fig. 1*c* and the step response of the proposed NLSMC scheme with initial and final damping ratios and settling time is displayed in Fig. 1*d*. From this step response, it can be seen that both peak overshoot and settling time are essentially low on account of the proposed NLSMC scheme

$$\frac{\mathrm{d}\boldsymbol{X}}{\mathrm{d}t} = A\boldsymbol{X} + B\boldsymbol{u}_{dq} + E\boldsymbol{v}_{dq} \tag{1}$$

$$\boldsymbol{y}_{dq} = C\boldsymbol{X} \tag{2}$$

where

$$\boldsymbol{X} = \left[i_d, i_q, V_{\mathrm{dc}}\right]^{\mathrm{T}},$$

$$A = \begin{bmatrix} -\dfrac{R_{\mathrm{f}}}{L_{\mathrm{f}}} & \omega & -\dfrac{u_d}{L_{\mathrm{f}}} \\ -\omega & -\dfrac{R_{\mathrm{f}}}{L_{\mathrm{f}}} & -\dfrac{u_q}{L_{\mathrm{f}}} \\ \dfrac{3u_d}{2C_{\mathrm{dc}}} & \dfrac{3u_q}{2C_{\mathrm{dc}}} & 0 \end{bmatrix}, \quad B = \begin{bmatrix} -\dfrac{V_{\mathrm{dc}}}{L_{\mathrm{f}}} & 0 \\ 0 & -\dfrac{V_{\mathrm{dc}}}{L_{\mathrm{f}}} \\ \dfrac{3i_{\mathrm{f}\_d}}{2C_{\mathrm{dc}}} & \dfrac{3i_{\mathrm{f}\_q}}{2C_{\mathrm{dc}}} \end{bmatrix},$$

$$E = \begin{bmatrix} \dfrac{1}{L_{\mathrm{f}}} & 0 \\ 0 & \dfrac{1}{L_{\mathrm{f}}} \\ 0 & 0 \end{bmatrix}, \quad C = \begin{bmatrix} 1 & 0 & 0 \\ 0 & 1 & 0 \\ 0 & 0 & 1 \end{bmatrix}$$

where $\boldsymbol{X}$, $\boldsymbol{u}_{dq}$, $\boldsymbol{v}_{dq}$ and $\boldsymbol{y}_{dq}$ represent the state-space vector, control input vector, input disturbance vector and control output vector, respectively. The switching function $\mathbb{S}_k$ of the kth leg of the VSC is defined as

$$\mathbb{S}_k = \begin{cases} 1 & \text{if } \mathbb{S}_k \text{ is on and } \mathbb{S}_k' \text{ is off} \\ 0 & \text{if } \mathbb{S}_k \text{ is off and } \mathbb{S}_k' \text{ is on} \end{cases} \tag{3}$$

Assume $v_{ck} = \mathbb{S}_k V_{\mathrm{dc}}$, switching state action u_{nk} is characterised as

$$u_{nk} = \left(\mathbb{S}_k - \frac{1}{3}\sum_{j=1}^{3}\mathbb{S}_j\right) \tag{4}$$

To acquire a quick dynamic response, the switching state functions u_d and u_q are defined from (1) as

$$\begin{aligned} u_d &= \frac{\lambda_d + L_{\mathrm{f}}\omega i_{\mathrm{f}\_q} + v_d}{V_{\mathrm{dc}}} \\ u_q &= \frac{\lambda_q - L_{\mathrm{f}}\omega i_{\mathrm{f}\_d}}{V_{\mathrm{dc}}} \end{aligned} \tag{5}$$

where $\lambda = (\mathrm{d}i_{\mathrm{f}}/\mathrm{d}t) + (R_{\mathrm{f}}/L_{\mathrm{f}})i_{\mathrm{f}}$.

The inputs u_d and u_q are consisted of linear decoupling compensation term and a non-linear term. To accomplish a quick dynamic response and zero steady-state errors, the non-linear sliding surface for the system is defined as

$$\begin{aligned} s(z,t) = I_{\mathrm{sp}} &= c^{\mathrm{T}}z(t) = \begin{bmatrix} c_1 & c_2 \end{bmatrix}\begin{bmatrix} z_1(t) \\ z_2(t) \end{bmatrix} \\ &= \begin{bmatrix} \boldsymbol{F} - \psi(y)A_{12}^{\mathrm{T}}p & 1 \end{bmatrix}\begin{bmatrix} z_1(t) \\ z_2(t) \end{bmatrix} \end{aligned} \tag{6}$$

where I_{sp} is the peak value of supply current, $\boldsymbol{F}$ is the linear gain matrix, $\psi(y)$ is the non-linear function, $\boldsymbol{P}$ is the positive-definite matrix and A_{12}^{T} can be defined from (1) by representing it to be a regular form [12]

$$A_{\mathrm{reg}} = \begin{bmatrix} A_{11} & A_{12} \\ A_{21} & A_{22} \end{bmatrix} \tag{7}$$

where

$$A_{11} = \begin{bmatrix} -\dfrac{R_{\mathrm{f}}}{L_{\mathrm{f}}} & \omega \\ -\omega & -\dfrac{R_{\mathrm{f}}}{L_{\mathrm{f}}} \end{bmatrix}, \quad A_{12} = \begin{bmatrix} -\dfrac{u_d}{L_{\mathrm{f}}} \\ -\dfrac{u_q}{L_{\mathrm{f}}} \end{bmatrix},$$

$$A_{21} = \begin{bmatrix} \dfrac{3u_d}{2C_{\mathrm{dc}}} & \dfrac{3u_q}{2C_{\mathrm{dc}}} \end{bmatrix}, \quad A_{22} = 0$$

The values of $z_1(t)$ and $z_2(t)$ of (6) are defined as

$$z_1(t) = x_1 y_1 \tag{8}$$

$$z_2(t) = x_2 y_2 \tag{9}$$

where x_1 is obtained from the average DC bus voltage V_{dc} and its reference value $V_{\mathrm{dc\_ref}}$

$$x_1 = v_{en} = V_{\mathrm{dc\_ref}(n)} - V_{\mathrm{dc}(n)} \tag{10}$$

and derivative of x_1 is defined as

$$x_2 = \dot{x_1} = \frac{1}{T}\left[v_e(n) - v_e(n-1)\right] \tag{11}$$

where T is the sampling time.

In sliding mode approach, the switching function values y_1 and y_2 are defined as follows:

$$\begin{aligned} y_1 &= +1 \quad \text{if } gx_1 > 0 \\ &= -1 \quad \text{if } gx_1 < 0 \\ y_2 &= +1 \quad \text{if } gx_2 > 0 \\ &= -1 \quad \text{if } gx_2 < 0 \end{aligned} \tag{12}$$

where g is the switching function$= c_3x_1 + c_4x_2$ and c_3, c_4 are constants.

The non-linear sliding surface defined in (6) is consisted of a linear and non-linear term. Primarily non-linear terms are zero and subsequently the linear term chooses initial damping ratio δ_1 and settling time t_{s}. From (6), $c_2 = 1$ and c_1 is defined as

$$c_1 = \boldsymbol{F} - \Psi(y)A_{12}^{\mathrm{T}}\boldsymbol{P} \tag{13}$$

Here $\boldsymbol{F}$ is designed for initial low damping ratio ($\delta_1 = 0.4$) and initial high settling time ($t_{\mathrm{s1}} = 0.25$) and matrix$\boldsymbol{F}$ can be found by using pole placement technique. Locations of the poles are at $\left(-\delta + \sqrt{\delta^2 - 1}\right)\omega_{\mathrm{n}}$ and $\left(-\delta - \sqrt{\delta^2 - 1}\right)\omega_{\mathrm{n}}$, where value of natural frequency of oscillation ω_{n} can be calculated from known values of the damping ratio δ and the settling time t_{s}. Thus ω_{n} can be written as $\omega_{\mathrm{n}} = 4/(\delta t_{\mathrm{s}})$. Accordingly poles of the close-loop system are

found to be placed at $-16 \pm 36.6606i$. Using pole placement technique, the gain matrix is found as $\boldsymbol{F} = [0.1738 \quad 0.9723]$. Considering final damping ratio as $\delta_2 = 0.86$ and settling time as $t_{s2} = 0.12$, the required gain matrix $\boldsymbol{k}_2$ can be computed as $\boldsymbol{k}_2 = [0.0804 \quad 0.9888]$ using pole placement technique.

The non-linear function $\psi(y)$ changes from 0 to $-\beta$ as output changes from its initial value to final value. It is given in [17] that introduction of this function changes the damping ratio of the system from its initial value (δ_1) to the final value (δ_2), where $\delta_2 > \delta_1$. When $\psi(y) = 0$ at $t = 0$, the damping ratio (δ_1) is contributed by $\boldsymbol{F}$. When its output reaches to the final value, the steady-state value of $\psi(y)$ becomes $\psi(y) = -\beta$, and the final damping ratio (δ_2) is contributed by $\boldsymbol{k}_2$, therefore $\psi(y)$ can be written as

$$\psi(y) = -\beta e^{-\bar{\alpha}y^2} \tag{14}$$

where $\bar{\alpha}$ is a positive constant that should have a large value to ensure a small initial value of ψ, y is the DC-link voltage and β is the tuning parameter, which is determined by the required gain of $\boldsymbol{k}_2$ and $\boldsymbol{F}$. Thus, the resulting equation is defined as

$$\boldsymbol{k}_2 = \boldsymbol{F} + \beta A_{12}^{\mathrm{T}} \boldsymbol{P} \tag{15}$$

To realise the desired damping ratio, the above equation can be equivalently expressed as

$$\beta = \frac{\boldsymbol{k}_2 - \boldsymbol{F}}{A_{12}^{\mathrm{T}} \boldsymbol{P}} \tag{16}$$

Equation (16) decides the value of β. This parameter helps to choose the damping ratio in conjunction with matrix$\boldsymbol{P}$, which is determined using linear matrix inequality technique based on the following equation:

$$(A_{11} - A_{12}\boldsymbol{F})^{\mathrm{T}} \boldsymbol{P} + \boldsymbol{P}(A_{11} - A_{12}\boldsymbol{F}) = -\boldsymbol{Q} \tag{17}$$

where $p \in R^{2\times 2}$ can be chosen based on the desired final damping ratio δ_2 and $\boldsymbol{Q}$ is the negative-definite matrix.

3 Stability of the sliding surface

Stability of the sliding surface is one of the important approaches in NLSMC design. Fig. 2*a* shows the sliding surface and its stability is determined by considering the NLSMC mode ($s(z, t) = 0$). From (6), the following expression can be obtained:

$$z_2(t) = -\boldsymbol{F} z_1(t) + \psi(y) A_{12}^{\mathrm{T}} \boldsymbol{P} z_1(t) \tag{18}$$

The system in regular form [12] can be described as

$$\dot{z}_1(t) = A_{11} z_1(t) + A_{12} z_2(t) \tag{19}$$

From (18) and (19), the system equation during NLSMC becomes

$$\dot{z}_1(t) = (A_{11} - A_{12}\boldsymbol{F} + \psi(y) A_{12} A_{12}^{\mathrm{T}} \boldsymbol{P}) z_1(t) \tag{20}$$

The stability of NLSMC technique is defined from the subsystem (20) by considering the theorem defined in [17]. Hence we apply the Lyapunov function to (20) to prove the stability of the system.

Let us consider the following Lyapunov function:

$$\dot{V}(t) = \dot{z}_1^{\mathrm{T}} \boldsymbol{P} z_1(t) + z_1^{\mathrm{T}}(t) \boldsymbol{P} \dot{z}_1(t) \tag{21}$$

By solving (21), it becomes

$$\dot{V}(t) = z_1^{\mathrm{T}}(t)[-\boldsymbol{Q} + 2\psi(y)\boldsymbol{P} A_{12} A_{12}^{\mathrm{T}} \boldsymbol{P}] z_1(t) \tag{22}$$

Therefore, by considering $\boldsymbol{P} A_{12} = \varepsilon$, (22) becomes

$$\dot{V}(t) = z_1^{\mathrm{T}}(t)[-\boldsymbol{Q} + 2\psi(y)\varepsilon\varepsilon^{\mathrm{T}}] z_1(t) \tag{23}$$

Since non-linear function $\psi(y)$ defined in (14) is negative and $\boldsymbol{P} A_{12} A_{12}^{\mathrm{T}} \boldsymbol{P} = \varepsilon\varepsilon^{\mathrm{T}} \geq 0$, the matrix $2\psi(y)\varepsilon\varepsilon^{\mathrm{T}}$ is a negative semi-definite. The matrix $-\boldsymbol{Q}$ is negative-definite and furthers the addition of a negative semi-definite and a negative-definite matrix results in a negative-definite matrix. Therefore, we can write $\dot{V}(t) < 0$, which satisfies the stability condition of NLSMC.

4 Proposed reference signal generation

The SRF-based control strategy is depicted in Fig. 2*b*. The SRF control method is one of the best methods for generation of reference signal during disturbance and uncertainty condition of power system network [18]. For generation of reference signal, the source voltages are applied to a phase-locked loop (PLL), where three phase unit vector signals and sine–cosine signals are generated as depicted in Fig. 2*c*. Three phase unit vector signals are transformed to $d - q - 0$ coordinate to obtain real component (u_d) and reactive component (u_q).

These components are multiplied with the peak amplitude of the source current (I_{sp}), generated using NLSMC scheme and get inverse transformed to $a - b - c$ coordinate for generating the source reference current. Compensating reference current (i_{f_ref}) is obtained by taking the difference between the load current and source reference current. For series converter, the reference voltage generation can be used for solving the voltage PQ problems. The control structure is primarily dependent on the integration of source voltage feed-forward ($V_{S(d-q)}$) and load voltage feedback ($V_{L(d-q)}$). The feed-forward controller delivers the essential transient response, and calculates the required compensating voltage (V_{scon_dq}) by taking the difference between the supply voltage (Vs_{d-q}) and load reference voltage ($V_{Load\_ref(d-q)}$). However, it does not consider voltage losses due to drop across the injection transformer and LC filter.

Therefore closed-loop voltage feedback compensation V_{Lc_dq} is added to minimise losses by passing the difference between load voltage ($V_{L(d-q)}$) and reference load voltage ($V_{Load\_ref(d-q)}$) through the PI controller ($k_p = 0.20$ and $k_i = 2.40$, refer the Appendix). These losses are added to the injected compensating voltage V_{scon_dq} to produce compensating reference voltage V_{scon_dq-ref} and finally inverse transformation is performed to obtain reference compensating voltages V_{scon_ref}.

5 Proposed switching dynamics in UPQC

5.1 Analysis of switching dynamics in shunt converter

Design of switching dynamics of shunt converter is a significant concern for controlling the switching band of hysteresis controller in transient condition. Instead of considering three-phase VSC, a single-phase VSC supported the DC-link capacitor is taken into account for simpler analysis. Fig. 3*a* shows schematic circuit for a single-phase shunt converter, and tracking of the reference current i_{faref} is presented in Fig. 3*b*.

The higher and lower boundary limits are generated by adding and deducting HBs for the compensating reference current. For tracing a positive reference current at particular time t', switch Q_1 is closed and Q_2 is opened, as a result of which capacitor voltage $(V_{dc}/2)$ is linked to converter, and also the reference current i_{fa}^{+} increases from $(i_{faref} - h)$ to $(i_{faref} + h)$. When it reaches a higher limit $(i_{faref} + h)$, the reference current i_{fa}^{-} needs to be fetched towards the lower band. To achieve this event, switch Q_1 is opened and Q_2 is closed and consequently capacitor voltage $(-V_{dc}/2)$ is coupled to the shunt converter for rising of negative reference current slope from instant t'' to t'''.

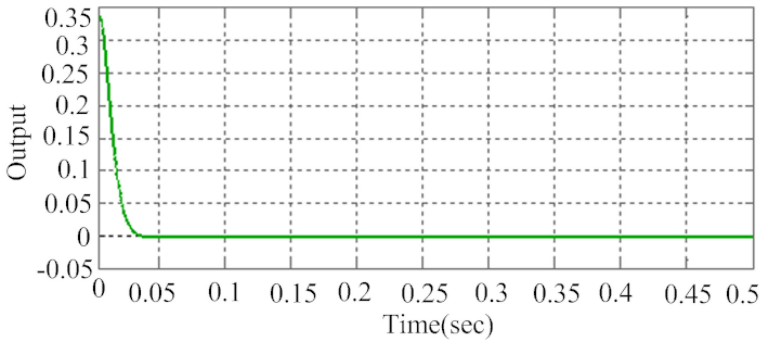

a

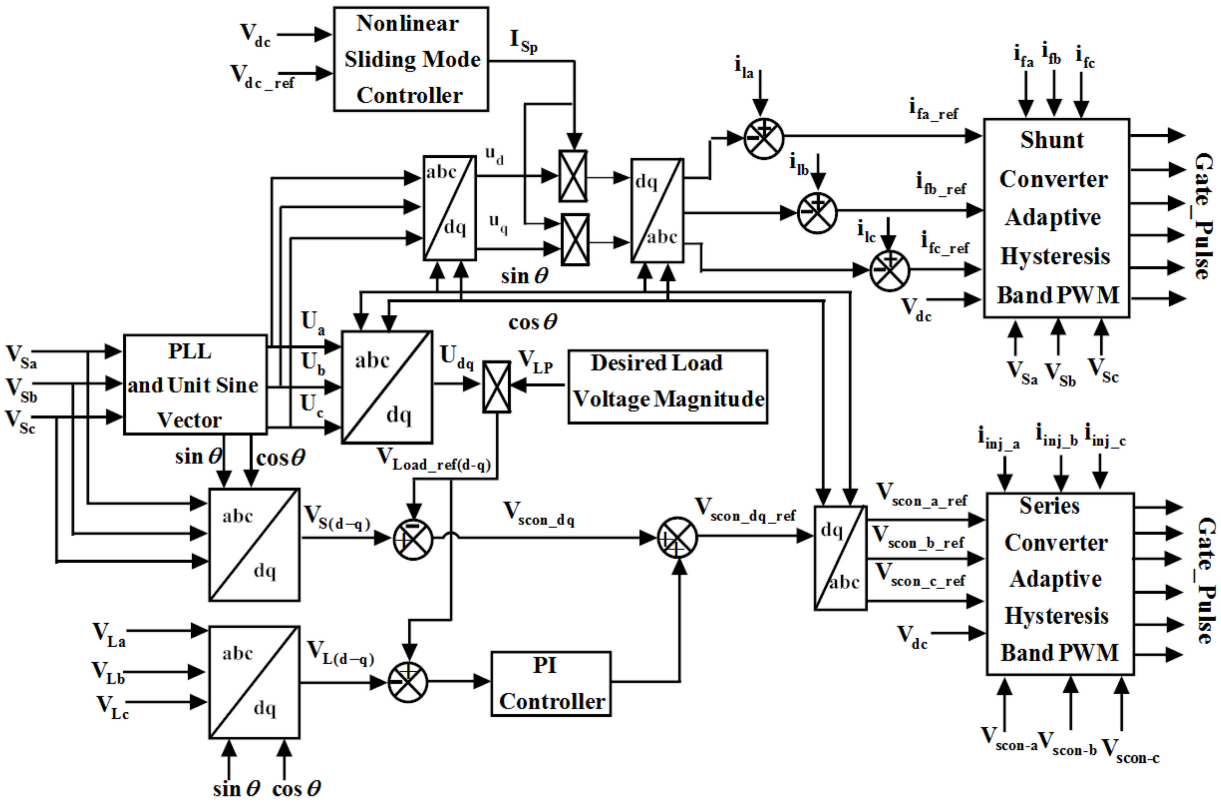

b

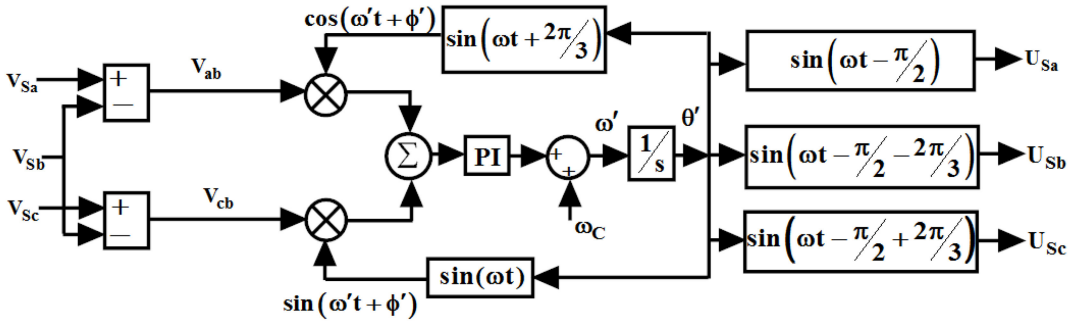

c

Fig. 2 *Sliding surface and control strategy for reference signal generation for UPQC*
(a) Sliding surface of proposed technique, ***(b)*** Proposed SRF-based control strategy for UPQC, ***(c)*** PLL circuit block diagram

For designing the switching band, we consider current waveform within a modulation cycle as shown in Fig. 3*b*. When switch Q_1 conducts, the corresponding voltage equation becomes

$$\frac{V_{\rm dc}}{2} - V_a - i_{\rm fa}R_{\rm fa} - L_{\rm fa}\frac{{\rm d}i_{\rm fa}}{{\rm d}t} = 0 \tag{24}$$

Thus

$$\frac{{\rm d}i_{\rm fa}}{{\rm d}t} = \frac{1}{L_{\rm fa}}\left(\frac{V_{\rm dc}}{2} - V_a - i_{\rm fa}R_{\rm fa}\right) \tag{25}$$

$$\frac{{\rm d}i_{\rm fa}}{{\rm d}t} = \frac{2{\rm HB}}{t_{\rm 1on}} \tag{26}$$

From Fig. 3*b*, the positive slope of the current for the duration t' to t'' is determined. Then on-time ($t_{\rm 1on}$) becomes

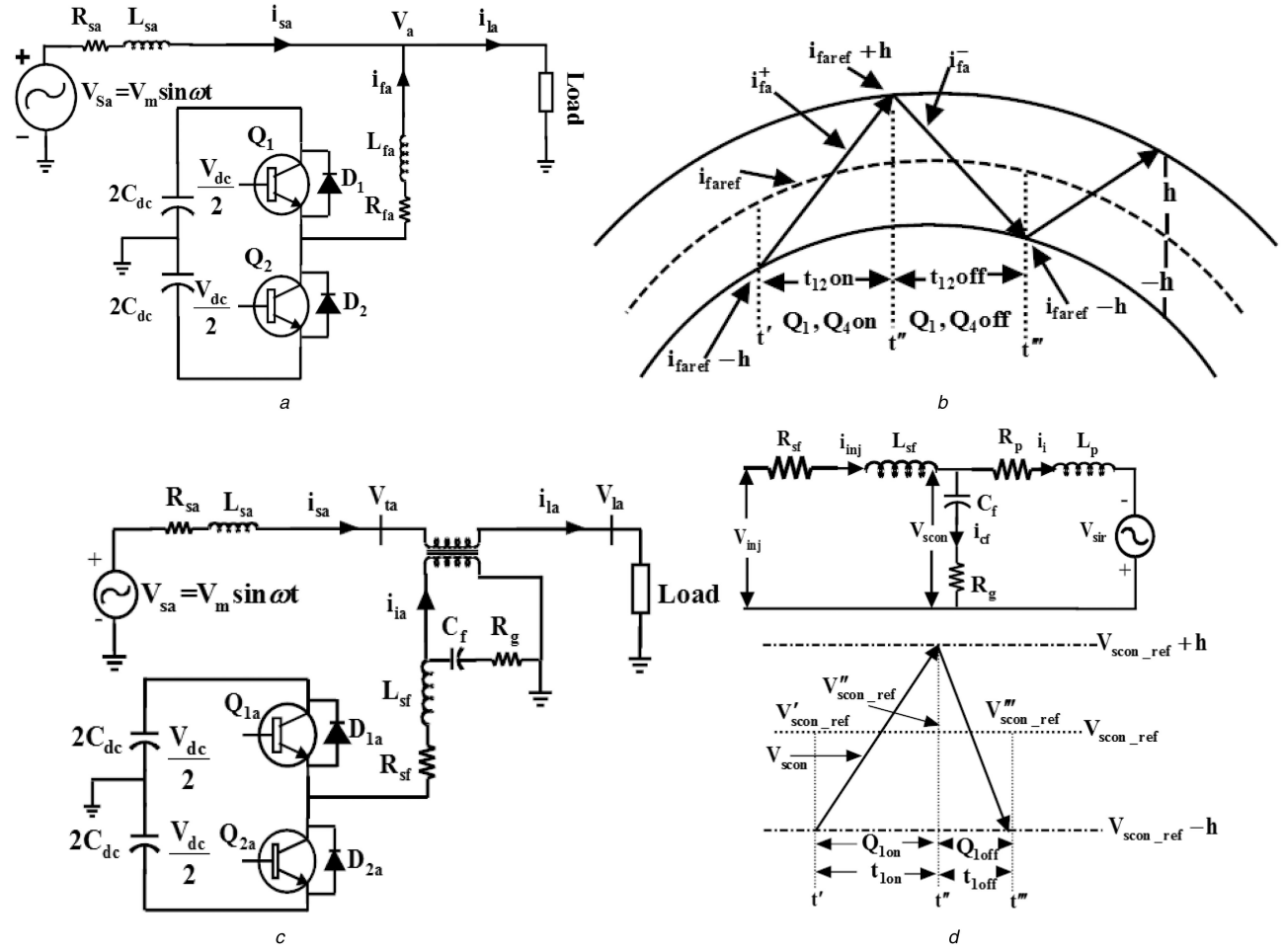

Fig. 3 *Switching dynamics analysis for the shunt and series converters*
(a) Schematic circuit of equivalent single-phase shunt converter, ***(b)*** Schematic diagram of switching dynamics for shunt converter, ***(c)*** Schematic circuit of equivalent single-phase series converter, ***(d)*** Equivalent circuit of series converter by exterior circuit and switching action of band control

$$t_{1\text{on}} = \frac{2\text{HB}}{\text{d}i_{\text{fa}}/\text{d}t} \tag{27}$$

Applying the value of $\text{d}i_{\text{fa}}/\text{d}t$ in (27), $t_{1\text{on}}$ becomes

$$t_{1\text{on}} = \frac{2\text{HB}L_{\text{fa}}}{(V_{\text{dc}}/2) - V_a - i_{\text{fa}} \cdot R_{\text{fa}}} \tag{28}$$

Similarly, when switch Q_2 conducts, the voltage equation becomes

$$-\frac{V_{\text{dc}}}{2} - V_a - i_{\text{fa}}R_{\text{fa}} - L_{\text{fa}}\frac{\text{d}i_{\text{fa}}}{\text{d}t} = 0 \tag{29}$$

Thus

$$\frac{\text{d}i_{\text{fa}}}{\text{d}t} = \frac{1}{L_{\text{fa}}}\left(-\frac{V_{\text{dc}}}{2} - V_a - i_{\text{fa}}R_{\text{fa}}\right) \tag{30}$$

The negative rise of current through the period t'' to t''' becomes

$$\frac{\text{d}i_{\text{fa}}}{\text{d}t} = \frac{-2\text{HB}}{t_{1\text{off}}} \tag{31}$$

Then off-time ($t_{1\text{off}}$) becomes

$$t_{1\text{off}} = \frac{-2\text{HB}}{\text{d}i_{\text{fa}}/\text{d}t} \tag{32}$$

Applying the value of $\text{d}i_{\text{fa}}/\text{d}t$ in (32), $t_{1\text{off}}$ becomes

$$t_{1\text{off}} = \frac{2\text{HB}L_{\text{fa}}}{(V_{\text{dc}}/2) + V_a + i_{\text{fa}}R_{\text{fa}}} \tag{33}$$

The switching frequency (f_c) is obtained by adding (28) and (33) (see (34)) Equation (35) can be obtained after simplifying (34)

$$f_c = \frac{1}{V_{\text{dc}}2\text{HB}L_{\text{fa}}}\left[\frac{V_{\text{dc}}^2}{4} - (V_a + i_{\text{fa}}R_{\text{fa}})^2\right] \tag{35}$$

From (35), we can obtain the HB

$$\text{HB} = \frac{1}{V_{\text{dc}}2f_cL_{\text{fa}}}\left[\frac{V_{\text{dc}}^2}{4} - (V_a + i_{\text{fa}}R_{\text{fa}})^2\right] \tag{36}$$

where V_a, V_{dc}, L_{fa} and i_{fa} are the source voltage, DC-link voltage, coupling inductor and compensating current, respectively. For

$$\begin{aligned} f_c &= \frac{1}{t_{1\text{on}} + t_{1\text{off}}} \\ &= \frac{1}{(2\text{HB}L_{\text{fa}}/((V_{\text{dc}}/2) - V_a - i_{\text{fa}}R_{\text{fa}})) + (2\text{HB}L_{\text{fa}}/((V_{\text{dc}}/2) + V_a + i_{\text{fa}}R_{\text{fa}}))} \end{aligned} \tag{34}$$

symmetrical operation of all three phases, it can be expected that HB profiles HB_a, HB_b, HB_c will almost be same, but have a phase difference.

5.2 Analysis of switching dynamics in series converter

The primary function of a series converter is to suppress the sag/swell, voltage harmonics and voltage unbalance from supply voltage. To accomplish this job accurately, the appropriate design of switching band is an important concern. The boundaries of switching band are created using a hysteresis band (h) as well as the reference voltage V_{ref}, the lower and higher boundaries are defined as ($V_{\text{ref}} + h$) and ($V_{\text{ref}} - h$), respectively.

To make the analysis easier, a single-phase series converter having a DC-link capacitor is taken into account as illustrated in Fig. 3*c*. A single-phase equivalent of series converter with exterior circuit parts is presented in Fig. 3*d*, where R_g is the switching band resistor, added in series with filter capacitor to make the switching band more linear in compared to the switching band present during only capacitor filter, V_{sir} is the equivalent voltage source and $Z_p = (R_p + \text{j}wL_p)$ is the equivalent impedance exterior to the series converter. To originate a relation involving switching frequency along with some additional parameters, one period of switching action is demonstrated in Fig. 3*d*. Since both positive and negative reference voltages are same for band control operation, we take into account first positive reference voltage.

When switch Q_{1a} is on, a positive DC-link voltage $+(V_{\text{dc}}/2)$ is applied over the filter elements. Applying Kirchhoff's voltage law and Kirchhoff's current law, the following equations are obtained:

$$L_{\text{sf}}\frac{\text{d}i_{\text{inj}}}{t_{\text{1on}}} = \frac{V_{\text{dc}}}{2} - R_{\text{sf}}i_{\text{inj}} - V_{\text{scon}} \tag{37}$$

$$\text{d}i_{\text{inj}} = \text{d}i_i + \text{d}i_{\text{cf}} \tag{38}$$

Injection current is slowly varied in nature in compared to the capacitor current. Thus variation of converter current is nearly equal to the variation in the capacitor current without losing accuracy. Thus (38) becomes

$$\text{d}i_{\text{inj}} = \text{d}i_{\text{cf}} \tag{39}$$

Rearranging the aforementioned equation for calculation of length of positive slope as

$$t_{\text{1on}} = \frac{L_{\text{sf}}\text{d}i_{\text{cf}}}{(V_{\text{dc}}/2) - R_{\text{sf}}i_{\text{inj}} - V_{\text{scon}}} \tag{40}$$

Further a negative slope is obtained by making the switch Q_{2a} on. This provides a converter output voltage as $-(V_{\text{dc}}/2)$. The series converter voltage is discharged through capacitor current to reach the lower limit of ($V_{\text{ref}} - h$). Similar to positive slope, the following equations are obtained for negative slope:

$$L_{\text{sf}}\frac{\text{d}i_{\text{inj}}}{t_{\text{1off}}} = \frac{V_{\text{dc}}}{2} + R_{\text{sf}}i_{\text{inj}} + V_{\text{scon}} \tag{41}$$

$$\text{d}i_{\text{inj}} = -\text{d}i_{\text{cf}} \tag{42}$$

$$t_{\text{1off}} = \frac{L_{\text{sf}}\text{d}i_{\text{cf}}}{(V_{\text{dc}}/2) + R_{\text{sf}}i_{\text{inj}} + V_{\text{scon}}} \tag{43}$$

Thus the complete time length of one switching period can be figured out as

$$T_{\text{sw}} = t_{\text{1on}} + t_{\text{1off}} = \frac{4V_{\text{dc}}}{V_{\text{dc}}^2 - (2R_{\text{sf}}i_{\text{inj}} + 2V_{\text{scon}})^2}L_{\text{sf}}\text{d}i_{\text{cf}} \tag{44}$$

Modification in capacitor current $\text{d}i_{\text{cf}}$ may be found from the capacitor dynamic equation

$$V_{\text{scon}} = \frac{1}{C_{\text{f}}}\int i_{\text{cf}}\,\text{d}t + R_g i_{\text{cf}} \tag{45}$$

Differentiating and relocating the aforementioned equation, the variation of the capacitor current could be defined as

$$\text{d}i_{\text{cf}} = \frac{1}{R_g}\left(\text{d}V_{\text{scon}} - \frac{i_{\text{cf}}t_{\text{1on}}}{C_{\text{f}}}\right) \tag{46}$$

As series converter voltage (V_{scon}) is excellently tracking reference voltage $(V_{\text{scon\_ref}})$, the series converter voltage corresponding to reference voltage is $V_{\text{scon}} = V_{\text{scon\_ref}}$.

Due to a negligible voltage drop across the capacitor at high frequency, the variation of capacitor voltage is minimised. Thus

$$\begin{cases} \text{d}V_{\text{scon}} = \left(V'_{\text{scon\_ref}} + h\right) - \left(V_{\text{scon\_ref}} - h\right) = 2\text{HB} \\ \dfrac{(i_{\text{cf}}t_{\text{1on}})}{C_{\text{f}}} = \text{d}V_{\text{cf}} = 0 \end{cases} \tag{47}$$

Substituting (47) into (46), the variation of capacitor current is procured as

$$\text{d}i_{\text{cf}} = \frac{2\text{HB}}{R_g} \tag{48}$$

Substituting (48) into (44), the time required for one switching period is obtained as

$$T_{\text{sw}} = \frac{L_{\text{sf}}8\text{HB}V_{\text{dc}}}{R_g\left[V_{\text{dc}}^2 - (2R_{\text{sf}}i_{\text{inj}} + 2V_{\text{scon}})^2\right]} \tag{49}$$

A fundamental component can only be assumed in the reference voltage and the switching frequency of the band controller can be expressed as

$$f_{\text{sw}} = \frac{R_g\left[V_{\text{dc}}^2 - 4(R_{\text{sf}}i_{\text{inj}} + V_{\text{scon}})^2\right]}{L_{\text{sf}}8\text{HB}V_{\text{dc}}} \tag{50}$$

From (50), it is perceived that the switching frequency relies on R_g/L_{sf} ratio, capacitor voltage, voltage drop in filter resistance, reference voltage and band (h). Simplifying (50) the HB for series converter is obtained by

$$\text{HB} = \frac{R_g}{V_{\text{dc}}2f_{\text{sw}}L_{\text{sf}}}\left[\frac{V_{\text{dc}}^2}{4} - (R_{\text{sf}}i_{\text{inj}} + V_{\text{scon}})^2\right] \tag{51}$$

6 Simulation result and discussion

To verify the effectiveness of UPQC, the proposed control strategy has been tested using MATLAB/SIMULINK with system parameters given in Table 1. The three-phase UPQC system comprises of shunt and series converters with a common DC-link capacitor. A three-phase diode-rectifier bridge feeding RL load is used as a harmonic current producing load with a total harmonic distortion (THD) of 32.3%. For simulation analysis, some assumptions have been considered such as a step change of load at 0.15 s for transient performance, 20% of sag/swell creation between 0.12 and 0.18 s for four cycles, source voltage harmonic creation by adding fifth and seventh harmonics to the source voltage and voltage unbalance formation by varying phase-A and phase-C amplitudes up to ±20 % from its nominal value. Here we consider two different cases for analysing the performance of UPQC.

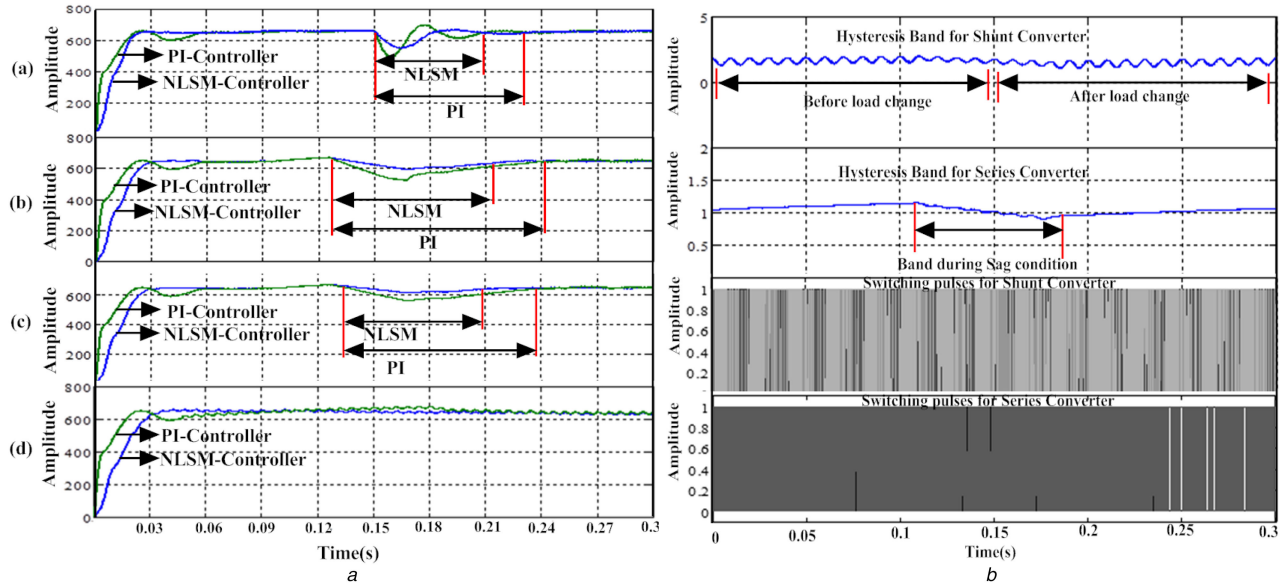

Fig. 4 *DC-link voltage with HB and corresponding switching patterns*
(a) Performance comparison of DC-link voltage using PI and NLSMC controllers, ***(b)*** HB and switching patterns for shunt and series converters

6.1 Case 1: DC-link voltage performance

In this case, the performance comparison of NLSMC and PI controllers for controlling the DC-link voltage of UPQC is considered. The comparison is based on the time required for stabilisation of DC-link voltage in the transient (load) and supply voltage disturbance conditions. The performance of the shunt converter of the UPQC for controlling the DC-link voltage with NLSMC and PI controllers for load transient, sag, swell and voltage unbalance conditions are given in Fig. 4*a* from top to bottom order. Gains of the PI controller (K_P and K_I) are tuned first for a ($R = 45\ \Omega, L = 35$ mH) based on [19] and the values of K_P and K_I are about 0.248 and 0.065, respectively. It is observed from the figure that, in case of the PI controller, the shunt converter takes almost 0.06 s to stabilise the DC-link voltage at the initial condition. When the load changes from $R = 45\ \Omega, L = 35$ mH to $R = 35\ \Omega, L = 25$ mH with a step time of 0.15–0.3 s, it almost takes 0.07 s to reach a steady state with some overshoot and undershoot. During the sag and swell conditions, the DC-link voltage falls down up to 560 and 570 V at 0.15 s from its reference value and takes 0.11 and 0.10 s, respectively, for stabilisation. In case of unbalance source voltage condition, the DC-link voltage slightly deviates from its reference value at 0.14 s and takes 0.05 s to stabilise.

In case of the proposed NLSMC, the DC-link voltage stabilises within 0.02 s at the initial stage, and at load transient condition, it takes about 0.04 s for stabilisation with low overshoot and low undershoot. In addition, the steady state ripples in DC-link voltage is negligible. Thus, it helps in reduction of steady-state distortion in source current. When sag and swell occur in supply side, DC-link voltage falls down to 590 and 600 V, respectively, at 0.15 s and takes about 0.08 and 0.07 s to stable. In unbalanced case, DC-link voltage cannot deviates from its original position and always follows the reference value. Thus, the proposed NLSMC controller technique enhances the performance of UPQC. Table 2 gives a comparison of the DC-link performance for PI and NLSMC controller schemes.

Table 1 System parameters

	Parameters	Notation	Value
source	voltage	V_{sabc}	360 V
	frequency	f	50 Hz
	resistor	R_s	1 Ω
	inductor	L_s	0.1 mH
load	diode rectifier		6-diode
	resistor	R_L	45 Ω
	inductor	L_L	35 mH
DC link	reference voltage	V_{dc_ref}	650 V
	capacitor	C_{dc}	4000 μF
shunt converter	interface inductor and resistor	(L_f, R_f)	2.5 mH and 0.5 Ω
	switching frequency	f_{sw}	10 kHz
series converter	AC filter inductor and capacitor	(R_{sf}, L_{sf}, C_f)	2 Ω, 2 mH and 6 μF
	switching band resistor	R_g	2 Ω
	injection transformer specification and inductance	L_j	7 : 1 turns ratio 4 mH

Table 2 Comparison of the PI and NLSMC controllers for DC-link voltage control performance

Type of conditions	PI, s	NLSMC, s
time required for stabilisation at initial stage	0.06	0.02
time required for stabilisation at load change	0.07	0.04
time required for stabilisation at sag condition	0.11	0.08
time required for stabilisation at swell condition	0.10	0.07
time required for stabilisation during unbalance supply condition	0.05	0

6.2 Case 2: Consideration of overall performance

In this section, we consider the overall operational performance of UPQC based on proposed control strategy. Fig. 4*b* shows the switching bands and switching patterns of both shunt and series converters of UPQC from top to bottom order.

For shunt converter, the band violation is negligible during load changing conditions, thus, tracking the performance of compensating current is improved with greater reduction of ripples in the source current. In case of series converter, band violation is less during sag condition and band voltage is almost linear. Thus, it improves the tracking performance of compensating voltage, which in turn leads to better compensation capability to load voltage. The compensating current and voltage tracking performances of PI with fixed hysteresis controller and proposed NLSM with new switching dynamics are sequentially presented in Fig. 5*a*. From the figure, it is clear that the proposed control strategy exhibits better tracking performance irrespective of disturbance occurring in load side or source side.

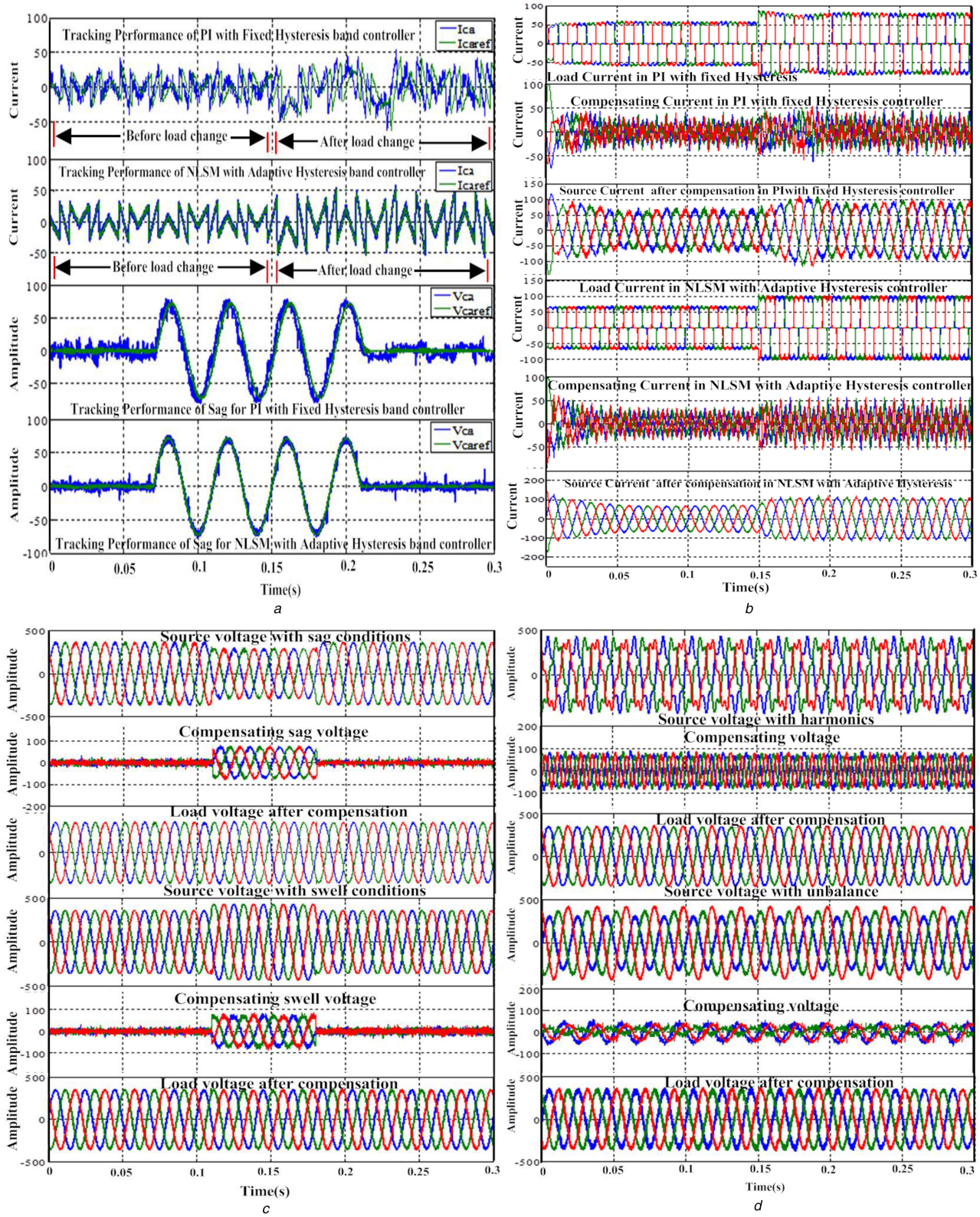

Fig. 5 *Simulation results for operating performance of the UPQC system*

(a) Tracking performance comparison of PI with fixed HB and NLSMC with new switching dynamics, ***(b)*** Performance of the shunt converter of the UPQC with (PI, NLSMC) and (conventional, new switching dynamics) for load perturbations, ***(c)*** Performance of series converter of UPQC during sag/swell condition using proposed control algorithm, ***(d)*** Performance of series converter of UPQC during harmonics (distorted) and unbalanced supply condition using proposed control algorithm

The performance of shunt converter is tested in Fig. 5*b* with load changing conditions and it is found that proposed NLSM shows better result as compared to PI with fixed hysteresis controller. The analysis is based on the THD. According to Table 3, THD of the source current before and after transient conditions are found to be 3.26 and 4.32%, respectively in conventional controller, whereas in the case of proposed controller they are reduced to 2.42 and 2.84%, respectively.

As compensating voltage contents switching ripple, it produces unnecessary distortion across the series transformer when it is injected through series transformer. According to Table 4, THD of the compensating voltage for sag and swell conditions are 4.24 and 4.13%, respectively, in conventional controller, whereas in the case of proposed controller they are reduced to 2.45 and 2.38%, respectively. Hence the proposed control strategy can enhance the compensation capability by reducing the amount of ripple in the

compensation voltage. Fig. 5*c* shows the sag/swell voltage compensation performance, where the series converter is utilised to compensate the load voltage around its nominal value by proper injection of compensating voltage through series transformer. Fig. 5*d* shows the compensation performance of series converter of UPQC for compensating harmonic voltage and unbalance source voltage. It is clear that, the proposed control strategy can satisfactorily eliminate all harmonics and unbalance present in the source voltage by injecting proper compensation voltage and makes the load voltage free from all such disturbances, which confirms the superiority of the proposed control strategy.

7 Result analysis using real-time HIL system

A real-time HIL system is configured to validate effectiveness of the proposed control strategy of UPQC. Fig. 6*a* shows the laboratory experimental setup using HIL system. The HIL simulation is a system that is utilised as a development and test of complex real-time embedded systems. The real-time HIL system consists of an OPAL-RT digital simulator (OP5600) with OP5142 Xilinx SPARTAN-3 (3xc3s5000) FPGA processor as shown in Fig. 6*b*.

The performance of the UPQC on the real-time HIL system is evaluated for load transient, voltage sag/swell, voltage unbalance, voltage harmonic and voltage interruptions conditions. For the experimental validation, we consider the same set of system parameters and load conditions as specified in simulation analysis. The details of load, compensating and source current under transient condition are presented in Fig. 7*a* for conventional and proposed controllers from top to bottom order. It is analysed from figure that, the source current waveform of proposed method is comparatively more sinusoidal than conventional PI with fixed hysteresis controller. Fig. 7*b* shows the waveform of voltage sag/swell with a depth of 20% and its corresponding source voltage, compensating voltage and load voltage after compensation, respectively, in a top to bottom order. As shown in the figure, the series converter of UPQC compensates the voltage sag/swell by injecting a voltage with proper amplitude and polarity. As a result, the load voltage is compensated completely.

Fig. 7*c* shows an experimental study of voltage harmonics and voltage unbalance compensation capability of the proposed algorithm from top to bottom order. The series converter of UPQC acts as a series-type harmonic voltage compensator to filter out harmonic components and provides quality voltage to the load. Similarly, in case of unbalanced supply voltage the series converter of the UPQC can inject a proper amount of voltage for regulating the load voltage to its nominal value. The performance of the DC-link voltage control is analysed under situation such as sudden load change, voltage sag/swell and supply voltage unbalance condition. Fig. 7*d* shows the DC-link voltage for both conventional PI and proposed controllers during these conditions are shown from top to bottom order. From the result, it is observed that the proposed control algorithm provides better voltage regulation in compared to the conventional PI controller. The performance of the series converter during voltage interruptions condition by using the proposed control algorithm is shown in Fig. 7*e*. The DC-link voltage, supply voltage, compensating voltage and load voltage after compensation with proposed method are shown in figure from top to bottom order, respectively. It is observed from the figure that, the DC-link capacitor voltage is able to settle down quickly and provides better voltage regulation in compared to the conventional PI controller. Correspondingly, the series converter of UPQC detects the voltage interruptions and injects the equal amount of voltages so that the load voltage is regulated to its nominal value.

Table 3 Comparison of source current THD for conventional and proposed control method

Type of condition	Before compensation, %	Compensation with UPQC	
		Conventional PI with fixed hysteresis controller, %	Proposed control method, %
source current THD before load changing	32.3	3.26	2.42
source current THD after load changing	32.3	4.32	2.84

Table 4 Compensating voltage THD Comparison for conventional and proposed control method

Different conditions	Conventional PI with fixed hysteresis controller, %	Proposed control method, %
compensating voltage THD during sag condition	4.24	2.45
compensating voltage THD during swell condition	4.13	2.38

8 Conclusions

A novel NLSMC technique along with new switching dynamics control strategy for UPQC is proposed in this paper to improve the PQ problems in power distribution network. It is observed from both simulation and experimental studies that, the NLSMC controller technique is superior to PI controller for controlling the DC-link voltage of UPQC, as it delivers less overshoot and less settling time for stabilising the DC-link voltage during occurrence

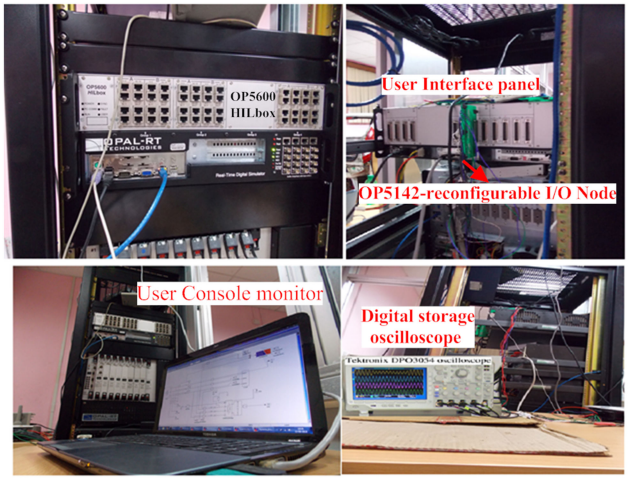

a

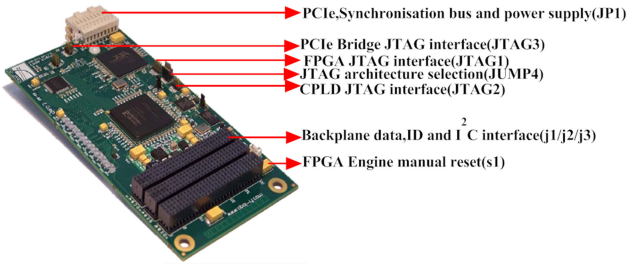

b

Fig. 6 *Laboratory experimental setup*
(a) Real-time HIL system, ***(b)*** OP5142 connectors and layout

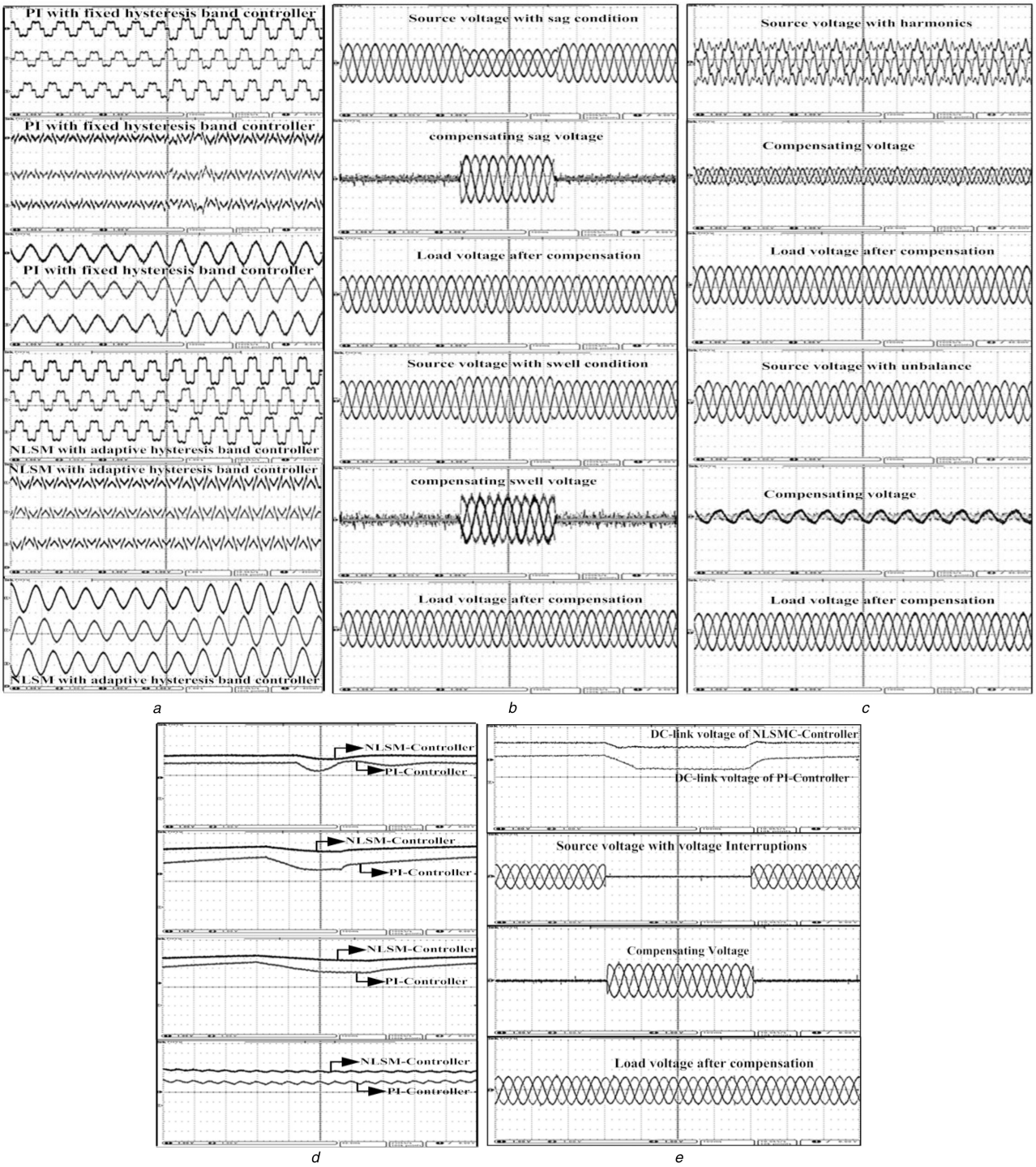

Fig. 7 *Real-time results*

(a) Load current, compensating current and source current (scale: 20 A/div), ***(b)*** Source voltage (scale: 120 V/div), compensation voltage (scale:60 V/div), load voltage (scale:120 V/div) under sag/swell condition, ***(c)*** Source voltage under distortion and unbalance condition (scale:120 V/div), compensation voltage under distortion and unbalance condition (scale: 40 V/div) and load voltage under distortion free and unbalance free condition (scale:120 V/div), ***(d)*** DC-link voltage, ***(e)*** DC-link voltage during voltage interruptions, source voltage during voltage interruptions (scale:130 V/div), compensating voltage during voltage interruptions (scale:130 V/div) and load voltage during voltage interruptions (scale:130 V/div)

of load transient, voltage sag/swell, voltage unbalance and voltage interruptions in the power distribution network. The performance of UPQC mainly depends upon how accurately and how quickly reference signals are derived. Hence, novel NLSMC-SRF-based control strategy is utilised in the UPQC system for quick extraction of the reference signal, which plays a significant role in the HB calculation.

The proposed switching dynamics control strategy generates the HB more accurately and makes the band calculation simpler. Consequently, this control strategy can overcome drawbacks of band violation and switching losses occurring in the fixed hysteresis band, in the presence of load as well as source perturbations. Therefore, the tracking performance of UPQC is improved, which drastically reduces the switching ripples present in the compensating voltage and source current. With the aforementioned views, it can be realised that the proposed NLSMC-SRF with switching dynamic for HB control strategy can enhance the performance of UPQC during power system dynamic conditions by eliminating PQ problems such as current/voltage harmonics, voltage sag/swell, voltage unbalance and voltage interruptions.

9 References

[1] Ketzer, M.B., Brandão, J.C.: 'Multivariable load current sensorless controller for universal active power filter', *IET Power Electron.*, 2014, **7**, (7), pp. 1777–1786

[2] Patjoshi, R.K., Mahapatra, K.K.: 'Performance analysis of shunt active power filter using PLL based control algorithms under distorted supply condition'. IEEE 2013 Students Conf. Engineering and Systems, 2013, pp. 1–6

[3] Shamsi-nejad, M.A., Khooban, M.H., Khalghani, M.R.: 'Dynamic voltage restorer control using bi-objective optimisation to improve power quality's indices', *IET Sci. Meas. Technol.*, 2014, **8**, (4), pp. 203–213

[4] Khadkikar, V.: 'Fixed and variable power angle control methods for unified power quality conditioner: operation, control and impact assessment on shunt and series inverter kVA loadings', *IET Power Electron.*, 2013, **6**, (7), pp. 1299–1307

[5] Heydari, H., Moghadasi, A.H.: 'Optimization scheme in combinatorial UPQC and SFCL using normalized simulated annealing', *IEEE Trans. Power Deliv.*, 2011, **26**, (3), pp. 1489–1498

[6] Teke, A., Saribulut, L., Tümay, M.: 'A novel reference signal generation method for power-quality improvement of unified power-quality conditioner', *IEEE Trans. Power Deliv.*, 2011, **26**, (4), pp. 2205–2214

[7] Mondal, S., Mahanta, C.: 'Nonlinear sliding surface based second order sliding mode controller for uncertain linear systems', *Commun. Nonlinear Sci. Numer. Simul.*, 2011, **16**, (9), pp. 3760–3769

[8] Khalick, A.El., Uchiyama, M.N., Sano, S.: 'Sliding mode contouring control design using nonlinear sliding surface for three-dimensional machining', *Int. J. Mach. Tools Manuf.*, 2013, **65**, pp. 8–14

[9] Huang, Y., Kuo, T.: 'Adaptive sliding-mode control for nonlinear systems with uncertain parameters', *IEEE Trans. Syst. Man Cyber.*, 2008, **38**, (2), pp. 534–539

[10] Cheng, G., Peng, K.: 'Robust composite nonlinear feedback control with application to a servo positioning system', *IEEE Trans. Ind. Electron.*, 2007, **54**, (2), pp. 1132–1140

[11] Lin, C., Liu, T., Wei, M.*, et al.*: 'Design and implementation of a chattering-free non-linear sliding-mode controller for interior permanent magnet synchronous drive systems', *IET Power Appl.*, 2012, **6**, (6), pp. 332–344

[12] Bandyopadhyay, B., Fulwani, D.: 'High-performance tracking controller for discrete plant using nonlinear sliding surface', *IEEE Trans. Ind. Electron.*, 2009, **56**, (9), pp. 3628–3637

[13] Khadem, S.K., Basu, M., Conlon, M.F.: 'Harmonic power compensation capacity of shunt active power filter and its relationship with design parameters', *IET Power Electron.*, 2014, **7**, (2), pp. 418–430

[14] Sasitharan, S., Mishra, M.K.: 'Constant switching frequency band controller for dynamic voltage restorer', *IET Power Electron.*, 2010, **3**, (5), pp. 657–667

[15] Rahmani, S., Al-Haddad, K., Kanaan, Y.: 'Two PWM techniques for single-phase shunt active power filters employing a direct current control strategy', *IET Power Electron.*, 2007, **1**, (3), pp. 376–385

[16] Zhou, K., Wang, D.: 'Relationship between space-vector modulation and three-phase carrier-based PWM: a comprehensive analysis', *IEEE Trans. Ind. Electron.*, 2002, **49**, (1), pp. 186–196

[17] Fulwani, D., Bandyopadhyay, B., Fridman, L.: 'Non-linear sliding surface: towards high performance robust control', *IET Control Theory Appl.*, 2012, **6**, (2), pp. 1–8

[18] Kesler, M., Ozdemir, E.: 'Synchronous-reference-frame-based control method for UPQC under unbalanced and distorted load conditions', *IEEE Trans. Ind. Electron.*, 2011, **58**, (9), pp. 3967–3975

[19] Rahmani, S., Mendalek, N., Al-Haddad, K.: 'Experimental design of a nonlinear control technique for three-phase shunt active power filter', *IEEE Trans. Ind. Electron.*, 2010, **57**, (10), pp. 3364–3375

10 Appendix

The design of PI controller for compensation the losses present in RLC filter and series transformer are based on plant transfer function $G_p(s)$ and PI-compensator transfer function $G_i(s)$.

$$G_p(s) = \frac{1}{s^2 L_{sf} C_f + (R_{sf} s C_f + R_g C_f)s + 1}$$

$$G_i(s) = k_p + \frac{K_i}{s}$$

The closed-loop transfer function $G_c(s)$ of the above equation is

$$G_c(s) = \frac{s + (k_i/k_p)}{s^3 + ((R_{sf} + R_g)s^2/L_{sf}) + ((k_p + 1)/L_{sf}C_f)s + (k_i/L_{sf}C_f)}$$

Based on desired characteristics polynomial $(s^2 + 2\delta\omega_n s + \omega_n^2)(s + \alpha\omega_n)$, k_p and k_i are found to be

$$k_p = L_{sf}C_f(1 + 2\alpha\delta)\omega_n - 1 \quad \text{and} \quad k_i = \alpha L_{sf} C_f \omega_n^3$$

where ω_n is the natural frequency, α is constant and σ is the damping coefficient.